

Unstable flip-flopping spinning binary black holes

Carlos O. Lousto and James Healy

*Center for Computational Relativity and Gravitation,
School of Mathematical Sciences, Rochester Institute of Technology,
85 Lomb Memorial Drive, Rochester, New York 14623*

(Dated: October 9, 2018)

We give a unified description of the flip-flop effect in spinning binary black holes and the anti-alignment instability in terms of real and imaginary flip-flop frequencies. We find that this instability is only effective for mass ratios $0.5 < q < 1$. We provide analytic expressions that determine the region of parameter space for which the instability occurs in terms of maps of the mass ratio and spin magnitudes (q, α_1, α_2) . This restricts the priors of parameter estimation techniques for the observation of gravitational waves from binary black holes and it is relevant for astrophysical modeling and final recoil computations of such binary systems.

PACS numbers: 04.25.dg, 04.25.Nx, 04.30.Db, 04.70.Bw

Introduction: Advanced LIGO [1] is now operational and on the verge of confirming General Relativity's predictions of gravitational waves from the merging of binary black holes (BBH) [2–4]. With the beginning of the Gravitational Wave Astronomy era, one of the most important tasks will be to determine the physical parameters of these BBH systems. Particularly challenging to model are highly precessing effects near merger. These effects depend strongly on the spin orientations and magnitudes of each individual black hole.

The strongest dynamical effect of the spins on the orbit of BBH is the hangup effect [5], that depending on the spin components along the orbital angular momentum (aligned or counteraligned) delays or prompts the merger of BBH with respect to the nonspinning case.

Two recent studies shed light on interesting effects of spin precession: i) the individual spin of a black hole may totally flip directions along the orbital angular momentum during the latest inspiral phase of the BBHs [6, 7] and ii) for certain antialigned configurations the black hole spin components along the orbital angular momentum are unstable under angular perturbations [8].

In this letter we provide a unified description of these two phenomena which gives new insight on the origin of the misalignment instability and confirms its existence in higher post-Newtonian expansions and full numerical simulations. We also discuss some of the consequences of this phenomenon for astrophysical modeling, gravitational waves parameter estimation, and computation of gravitational recoils.

Post Newtonian spin dynamics: Gerosa et al. [8] have found that a binary black hole configuration with the larger black hole spin along the orbital angular momentum \vec{L} and the smaller hole spin counteraligned to it is unstable under polar angular perturbations when their separation is in between $r_{ud\pm} = (\sqrt{\alpha_2} \pm \sqrt{q\alpha_1})^4 M / (1 - q)^2$. This result was found using orbit averaging [9], an effective low post-Newtonian order technique. Here we

perform a study of these spin dynamics by numerically integrating higher post-Newtonian (3.5PN) equation of motion and spin evolutions (2.5PN) as given in [10, 11].

Each panel of Fig. 1 displays the results of 121 integrations of the PN spin and equations of motion for a labeled mass ratio $q = m_1/m_2 < 1$ and covering the $-1 \leq \alpha_{1L} \leq 0$ and $0 \leq \alpha_{2L} \leq 1$ quadrant of the aligned spin parameter space (except $q = 0.95$ which has 76 integrations.) The integrations start from quasi-circular orbits at a large enough initial binary separation such that the spins are stable, ie $r/M > R_c$ given in Eq. (3) (with the total mass of the system $M = m_1 + m_2$), and we stop at a fiducial $r = 11M$. We choose the spin of the large black hole $\vec{S}_2 = \alpha_2 m_2^2$ initially aligned with the orbital angular momentum \vec{L} and the spin of the smaller black hole $\vec{S}_1 = \alpha_1 m_1^2$ one degree from exact anti-alignment, i.e. 179 degrees from the \hat{L} -direction (we also tried 5 and 8 degrees misalignments). The instability occurs either when the larger or the smaller (or both) black hole spin is slightly misaligned with \hat{L} . The instability depopulates the upper left corner of the spin parameter space, with successively larger portions from $q = 0.5$ to $q = 1$, and strongly changes the spin components along \hat{L} bringing the binary system to strong precession.

From the initial large separations, when the system is stable and spins oscillate at the flip-flop frequency, Ω_{ff} , the binary separation shrinks due to gravitational radiation and eventually reaches a critical separation, see upper panel in Fig. 2. At this point the polar oscillations of the spin begin to grow fast in an out-spiral fashion (see lower panels).

As seen in the middle panels of Fig. 2, the spin misalignment reaches large values at later times (and smaller separations), but the cosine of the angles θ_{1L} and θ_{2L} that the spins form with \hat{L} -direction bare a relation that preserves (mostly) $\vec{S}_0 \cdot \hat{L}$ as expected [12], i.e. $q \cos \theta_{1L} + \cos \theta_{2L} = 1 - q$.

We will show next that the critical radii separating the

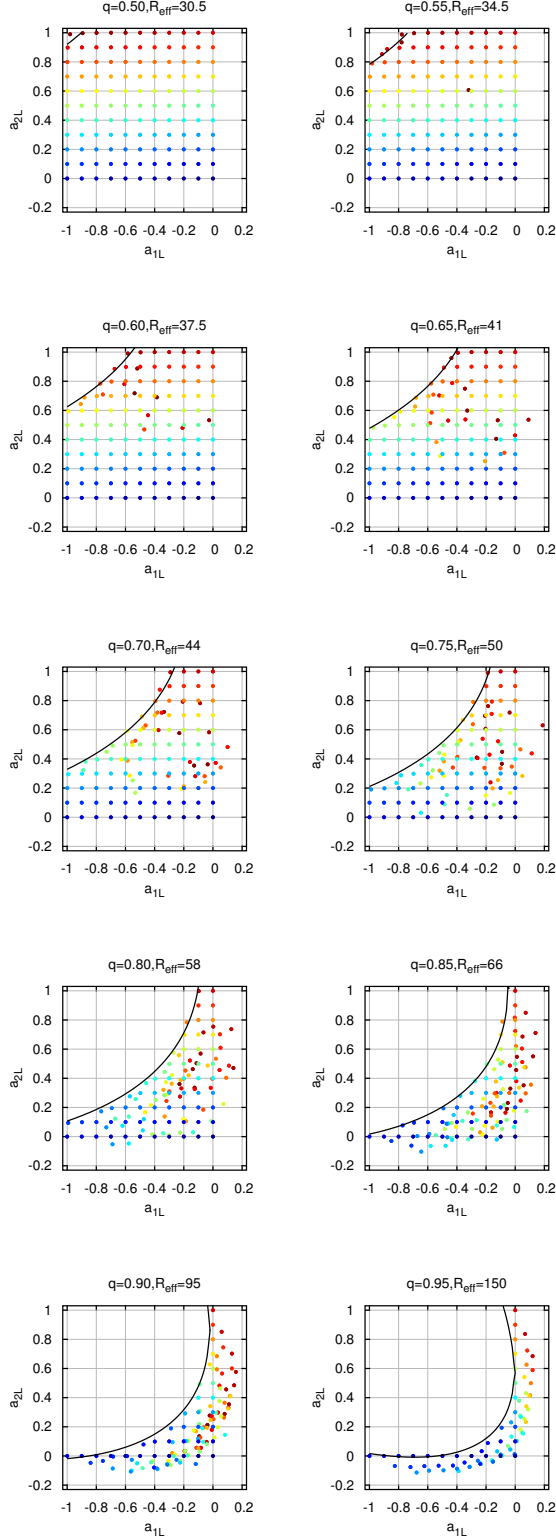


FIG. 1. Snapshots of the spin components along the orbital angular momentum at a binary separation $r/M = 11$. The integration of the PN evolution equations for each binary mass ratio q , started at $r/M > R_c$ with a uniform distribution of spins in the range $0 \leq \alpha_{2L} \leq 1$ for the large BH and $-1 \leq \alpha_{1L} \leq 0$ for the small BH, which was antialigned with the orbital angular momentum by 179-degrees. The color indicates the original value of the spins. The black curve models the depopulation region as given in Eq. (4).

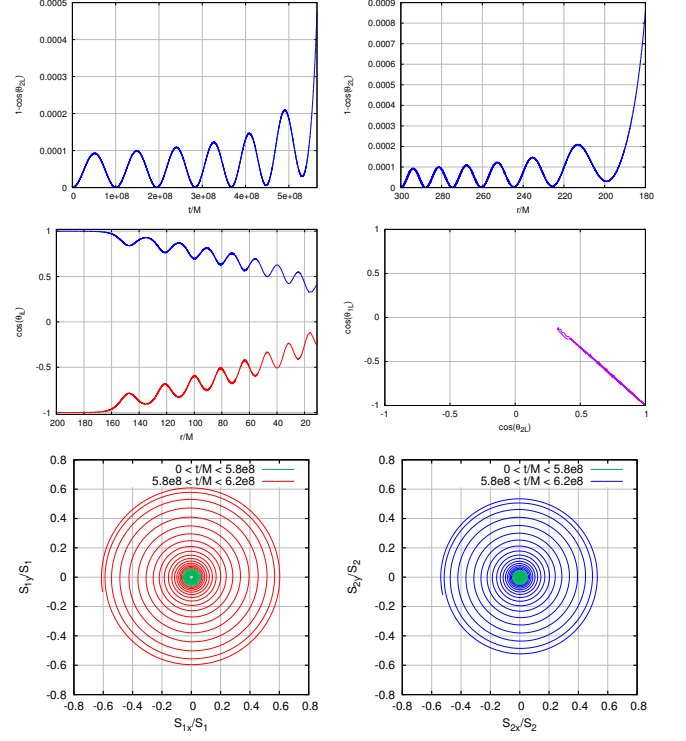


FIG. 2. Evolution of a binary with mass ratio $q = 0.75$, large BH spin $\alpha_{2L} = 1$ initially aligned and small BH spin $\alpha_{1L} = -1$ antialigned with the orbital angular momentum by 179-degrees. The upper panels display the onset of the instability from stable flip-flop oscillations. The middle panels display the development of the instability as the binary separation shrinks. Here $\cos \theta_{iL} = S_{iL}/S_i$ with $i = 1, 2$ for the small, large holes. The lower panels display a polar view of the onset of the misalignment instability.

two regimes can be described in terms of the vanishing of the *flip-flop* frequency, separating real and imaginary values, and corresponding to stable and unstable phases respectively.

Flip-Flop instability: In Ref. [7] we give the following expression for the *flip-flop* frequency; the frequency of polar oscillations (with respect to \hat{L}) of the spins in a binary system

$$\Omega_{ff}^2 = \frac{9}{4} \frac{(1-q)^2 M^3}{(1+q)^2 r^5} + 9 \frac{(1-q)(S_{1\hat{L}} - S_{2\hat{L}})M^{3/2}}{(1+q)r^{11/2}} - \frac{9}{4} \frac{(1-q)(3+5q)S_{1\hat{L}}^2}{q^2 r^6} + \frac{9}{2} \frac{(1-q)^2 S_{1\hat{L}} S_{2\hat{L}}}{qr^6} + \frac{9}{4} \frac{(1-q)(5+3q)S_{2\hat{L}}^2}{r^6} + \frac{9}{4} \frac{S_0^2}{r^6} + 9 \frac{(1-q)^2 M^4}{(1+q)^2 r^6}, \quad (1)$$

where $\vec{S}_0/M^2 = (1+q) [\vec{S}_1/q + \vec{S}_2]$.

The instability of Ref. [8] can be interpreted in terms of an *imaginary flip-flop* frequency, when the oscillations become exponentially growing modes. In fact, we see in Fig. 2 that at large separations the binary oscillates at

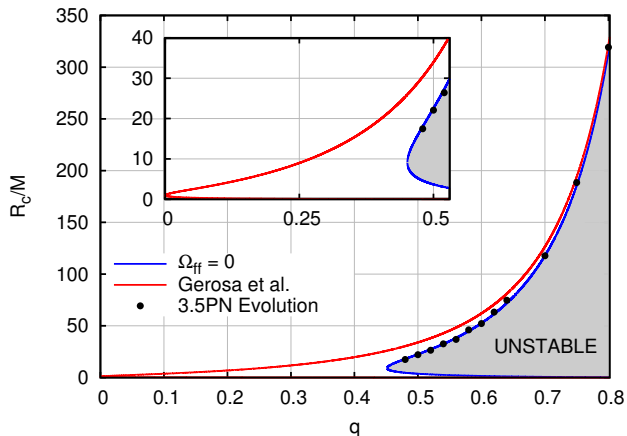


FIG. 3. The instability region, between R_c^\pm , as a function of the mass ratio, q , as the binary transitions from real to imaginary flip-flop frequencies (blue curve) for maximal spins $\alpha_{1L} = -1$ and $\alpha_{2L} = +1$. For comparison also plotted are $r_{ud\pm}$ from [8] (red curve). The dots correspond to 3.5PN evolutions.

the frequency given in Eq. (1). Thus the critical radius, R_c , for which the onset of the instability occurs satisfies

$$\Omega_{ff}(q, \vec{\alpha}_1, \vec{\alpha}_2, R_c) = 0. \quad (2)$$

The solution of this quadratic equation for antialigned spins leads to two roots R_c^\pm .

$$R_c^\pm = 2M \frac{A \pm 2(\alpha_{2L} - q^2 \alpha_{1L})\sqrt{B}}{(1 - q^2)^2}, \quad (3)$$

$$A = (1 + q^2)(\alpha_{2L}^2 + q^2 \alpha_{1L}^2),$$

$$-2q(1 + 4q + q^2)\alpha_{1L}\alpha_{2L} - 2(1 - q^2)^2$$

$$B = 2(1 + q) [(1 - q)q^2 \alpha_{1L}^2 - (1 - q)\alpha_{2L}^2$$

$$- 2q(1 + q)\alpha_{1L}\alpha_{2L} - 2(1 - q)^2(1 + q)].$$

We display this in Fig. 3 for the case of maximally spinning holes, i.e. $\alpha_{1L} = -1$ and $\alpha_{2L} = +1$, as a function of the mass ratio q as this case leads to the most unstable configuration (see Fig. 1). The instability occurs only above a given mass ratio, and in practice this leads to deviations for $q > 1/2$. There is no solution for instabilities in the other quadrants, thus they only occur when the small black hole is near anti-alignment and the large black hole is near alignment with \vec{L} .

We also verified that the large oscillations shown in the middle panels of Fig. 2, after the instability brought the spins to strong misalignments, are due to the frequency (1) becoming real again, and then back to imaginary successively.

We can now determine analytically the border between stable and unstable configurations in the spin parameter space. For a given q , there is a minimal R_c for which the instability has enough time to act and change the components of the spins along \hat{L} . We call this minimal radius R_{eff} . By inserting $r/M = R_{eff}$ into equation (2) we can solve the resulting quadratic equation for $\alpha_2^B(q, \alpha_{1L}) = \alpha_2^\pm(q, \alpha_{1L}; R_{eff})$

$$\alpha_2^B(q, \alpha_1) = \frac{(1 - q^2)\sqrt{R_{eff}} - q(1 + q^2)\alpha_{1L}}{3 - q^2} \mp \frac{1}{2} \frac{(1 - q^2)}{(3 - q^2)} \sqrt{C}, \quad (4)$$

$$C = 16q^2 \alpha_{1L}^2 - 2(1 - q^2)R_{eff} + 8(q^2 - 3),$$

$$- 8q\sqrt{R_{eff}}(1 + 2q - q^2)\alpha_{1L}/(1 - q).$$

Applying this formula to the border of the depopulated regions in Fig. 1 leads to a simple fit to all q -cases studied giving $R_{eff} = (26.2 - 18.6q)/(1 - q)$. This R_{eff} is larger for $q \sim 1$ than for $q \sim 1/2$ since the smaller the mass ratio the longer it takes radiation reaction to shrink the binary as the energy radiated near merger scales roughly with $\eta^2 = q^2/(1 + q)^4$ [13]. This shows that the instability acts on a radiation reaction time scale (bringing the binary towards merger) rather than the shorter precession time scale (or the much shorter orbital scale). We observe that above $q = 0.85$ the second root α_2^B , begins to also limit the upper part of the panel. In the $q = 1$ limit the two α_2^\pm roots agree, merging into a diagonal straight line, representing the fact that there is no instability for $q = 1$, i.e. only flip-flop oscillations with $\Omega_{ff}(q = 1) = \frac{3}{2} \frac{S_0}{r^3}$ (see Eq. (2)).

We thus obtain an analytic expression for the portion of the aligned spin binaries parameter space that the instabilities remove from an initial uniform distribution. These priors affect the conditional probability distribution and have consequences for the determination of posteriors distributions of parameter estimation techniques applied to binary black hole candidates to be observed by advanced LIGO [1].

Full Numerical Evolutions: Post-Newtonian evolutions do not accurately account for the final plunge, merger and ringdown of binary black holes. We hence stopped our PN evolutions at a fiducial separation of $r = 11M$. We have then performed a few representative full numerical simulations using the techniques in [3] to follow up those post-Newtonian integrations. The details of the five simulations are given in Table I.

Table II displays the properties of the final black hole remnant formed after merger. Notably, the measured recoil is very different from that expected if the spins would remain aligned (this prediction based on the formulae in [13]). The differences are not only due to the magnitude of the recoil, but notably, the velocity component along the original orbital angular momentum, which vanishes for the aligned spins configuration, now becomes the largest. Differences

TABLE I. Initial data parameters and system details for full numerical evolutions. The initial coordinate separation is $D = 11M$ and the intrinsic spins are $\alpha_{1,2}^{x,y,z}$. The eccentricity measured at the end of the inspiral is e_f , and the number of orbits just before merger N . # labels the PN runs that started at binary separation $r = 500M$ with normalized spins (a_1^z, a_2^z) .

#	(a_1^z, a_2^z)	q	α_1^x	α_1^y	α_1^z	α_2^x	α_2^y	α_2^z	N	e_f
1	(-0.8, 0.8)	0.70	0.7738	0.1876	-0.0775	0.6162	0.4183	0.2921	8.7	0.0037
2	(-0.4, 0.8)	0.75	-0.3205	0.2392	0.0070	-0.5926	-0.2040	0.4971	9.6	0.0009
3	(-0.6, 0.6)	0.75	0.5467	0.2462	-0.0223	0.4724	0.3311	0.1651	8.4	0.0024
4	(-0.8, 0.8)	0.75	0.0559	0.7598	-0.2440	-0.2564	0.6676	0.3585	8.6	0.0052
5	(-0.8, 0.4)	0.75	-0.4617	-0.4859	-0.4367	0.0581	-0.3765	0.1220	7.4	0.0040

TABLE II. Remnant properties of the merged black hole. The final mass m_{rem} and spin α_{rem} (normalized to total initial mass) are measured from the horizon, and the recoil velocity (in km/s) is calculated from the gravitational waveforms. Comparison with predicted aligned spins values m_{pre} , $\alpha_{pre}^{x,y,z}$, V_{pre}^{xy} , is based on [13]

#	m_{rem}	m_{pre}	α_{rem}^x	α_{rem}^y	α_{rem}^z	α_{pre}^z	V_{rem}^x	V_{rem}^y	V_{rem}^z	V_{pre}^{xy}
1	0.9445	0.9456	0.2712	0.1445	0.7464	0.7742	-3.9	28.7	-133.7	260.7
2	0.9408	0.9409	-0.1920	-0.0451	0.7909	0.7994	273.5	-24.9	-775.8	187.7
3	0.9485	0.9486	0.1994	0.1155	0.7216	0.7388	138.1	-11.2	557.8	200.4
4	0.9468	0.9462	-0.0685	0.2650	0.7591	0.7601	5.9	117.0	241.7	282.9
5	0.9534	0.9546	-0.0610	-0.1458	0.6683	0.6752	47.6	-11.1	386.4	201.7

are also observed in the final spin magnitude and orientation, less notable are the differences in the total energy radiated.

Discussion: We have provided a unified description of the polar oscillations and instabilities of the black hole spins in a binary system. Analytic expressions for the radius of the onset of instabilities and the region of parameter space affected by instabilities are also given. These expressions lead to restrictions of the prior distributions of aligned spins affecting the parameter estimations of gravitational wave observations from binary black holes by removing the unstable region from the posterior probability distributions. Further studies are required to quantify the effect in generic, precessing binaries.

In most cases the instabilities start affecting the binary before it enters the gravitational wave detectors sensitivity band, i.e. above 10Hz, [1]. For instance, in the limiting $q = 1/2$ case, when $R_{eff} \approx 30.5$, the binary's orbital frequency $\Omega_{orbit} = 2 \times 10^5 R_{eff}^{-3/2} (M_\odot/M) \text{Hz}$, leads to gravitational wave frequencies above 10Hz only for total binary masses (in solar masses units M_\odot) below $38M_\odot$. All other cases studied here are even less restrictive.

The spin instabilities in binary black hole systems studied here may also lead to larger gravitational recoils than expected from their almost counteraligned precursors. Thus, it is possible for accretion [14, 15] to anti-align spin binaries at large separations and then at smaller separations the binary spin alignment becomes unstable leading to black hole remnants acquiring thousand of km/s recoil velocities.

The authors would like to thank M. Campanelli, H. Nakano, V. Raymond, R. O'Shaughnessy, and Y. Zlochower for comments on the original manuscript. Authors also gratefully acknowledge the NSF for financial support from Grant PHY-1305730. Computational resources were provided by XSEDE allocation TG-PHY060027N, and by the BlueSky Cluster at Rochester Institute of Technology, which were supported by NSF grant No. AST-1028087, and PHY-1229173.

- [1] J. Aasi *et al.* (LIGO Scientific), *Class. Quant. Grav.* **32**, 074001 (2015), arXiv:1411.4547 [gr-qc].
- [2] F. Pretorius, *Phys. Rev. Lett.* **95**, 121101 (2005), gr-qc/0507014.
- [3] M. Campanelli, C. O. Lousto, P. Marronetti, and Y. Zlochower, *Phys. Rev. Lett.* **96**, 111101 (2006), gr-qc/0511048.
- [4] J. G. Baker, J. Centrella, D.-I. Choi, M. Koppitz, and J. van Meter, *Phys. Rev. Lett.* **96**, 111102 (2006), gr-qc/0511103.
- [5] M. Campanelli, C. O. Lousto, and Y. Zlochower, *Phys. Rev.* **D74**, 041501(R) (2006), gr-qc/0604012.
- [6] C. O. Lousto and J. Healy, *Phys. Rev. Lett.* **114**, 141101 (2015), arXiv:1410.3830 [gr-qc].
- [7] C. O. Lousto, J. Healy, and H. Nakano, (2015), arXiv:1506.04768 [gr-qc].
- [8] D. Gerosa, M. Kesden, R. O'Shaughnessy, A. Klein,

- E. Berti, U. Sperhake, and D. Trifirò, *Phys. Rev. Lett.* **115**, 141102 (2015), arXiv:1506.09116 [gr-qc].
- [9] J. D. Schnittman, *Phys. Rev.* **D70**, 124020 (2004), arXiv:astro-ph/0409174.
- [10] T. Damour, P. Jaranowski, and G. Schafer, *Phys. Rev.* **D77**, 064032 (2008), arXiv:0711.1048 [gr-qc].
- [11] A. Buonanno, Y. Chen, and T. Damour, *Phys. Rev.* **D74**, 104005 (2006), gr-qc/0508067.
- [12] E. Racine, *Phys. Rev.* **D78**, 044021 (2008), arXiv:0803.1820 [gr-qc].
- [13] J. Healy, C. O. Lousto, and Y. Zlochower, *Phys. Rev.* **D90**, 104004 (2014), arXiv:1406.7295 [gr-qc].
- [14] T. Bogdanović, C. S. Reynolds, and M. C. Miller, *Astrophys. J.* **661**, L147 (2007), arXiv:astro-ph/0703054.
- [15] M. Coleman Miller and J. H. Krolik, *Astrophys. J.* **774**, 43 (2013), arXiv:1307.6569 [astro-ph.HE].